SI for 'Microsecond resolution of cavitation bubble dynamics using a high-speed electrochemical impedance approach'

Figure S1 shows a schematic representation of the approach applied to the data acquisition and processing employed to extract the uncompensated resistance, the capacitance and the Faradaic current from the current time data and original voltage perturbation applied to the electrode.

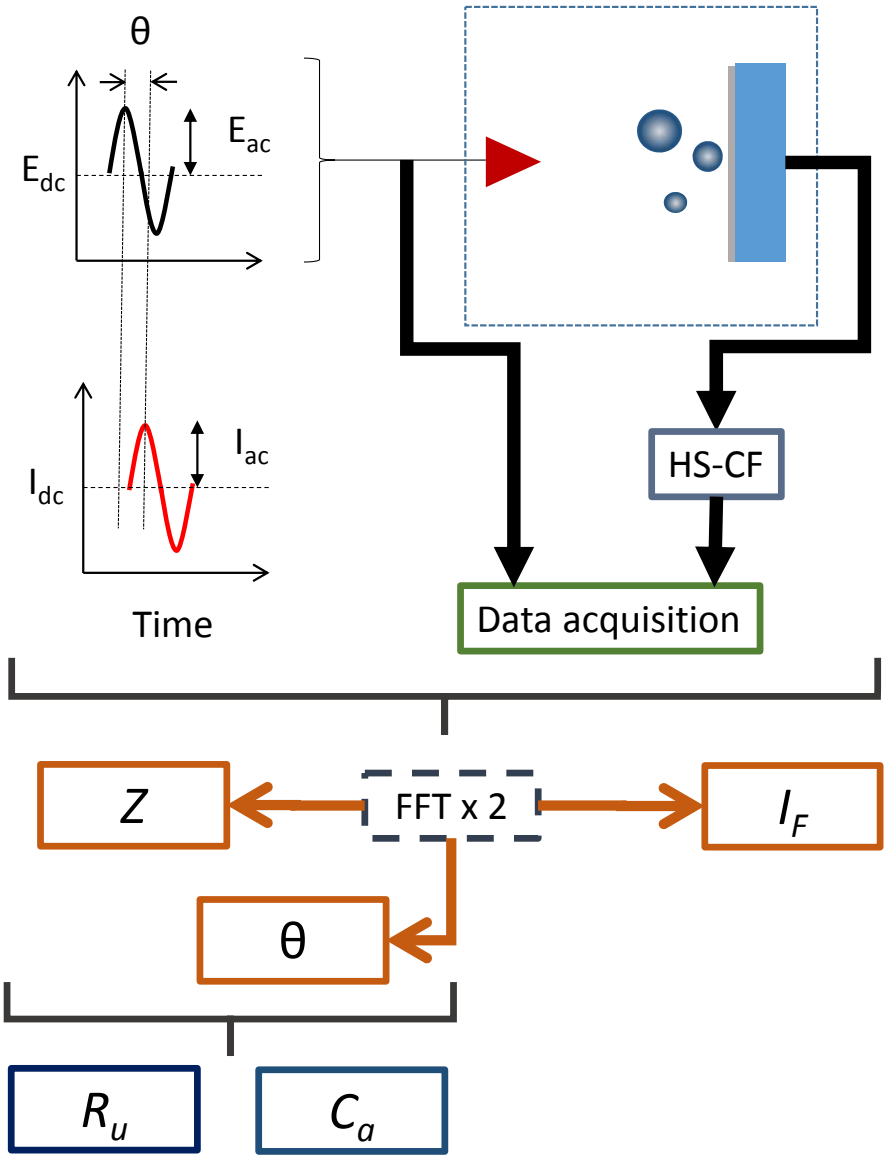

Figure S1. Schematic showing the approach adopted for the acquisition of data as cavitation events are generated at the electrode surface. Here E_{dc} represents the time averaged potential of the electrode with respect to the reference, E_{ac} represents the AC amplitude used (here 100 mV zero-to-peak), I_{dc} the time averaged current over the time window employed (here 2 µs), I_{ac} the amplitude of the AC current, θ the phase angle between the applied voltage perturbation and the resultant current, HS-CF the high speed current follower, Z the impedance, I_F the Faradaic current determined from the DC component returned from the FFT analysis of the current time signal, R_u the measured uncompensated resistance and C_a the apparent capacitance of the electrode.

The data collected in each experiment is analysed using an FFT approach. This enables the amplitudes and associated phases of the frequency components to be determined as well as the 'DC' (or Faradaic)

current during the time window employed (here 2 µs). Figure S2 shows an example of the output of the FFT analysis when applied to the voltage (a) and current signal (b).

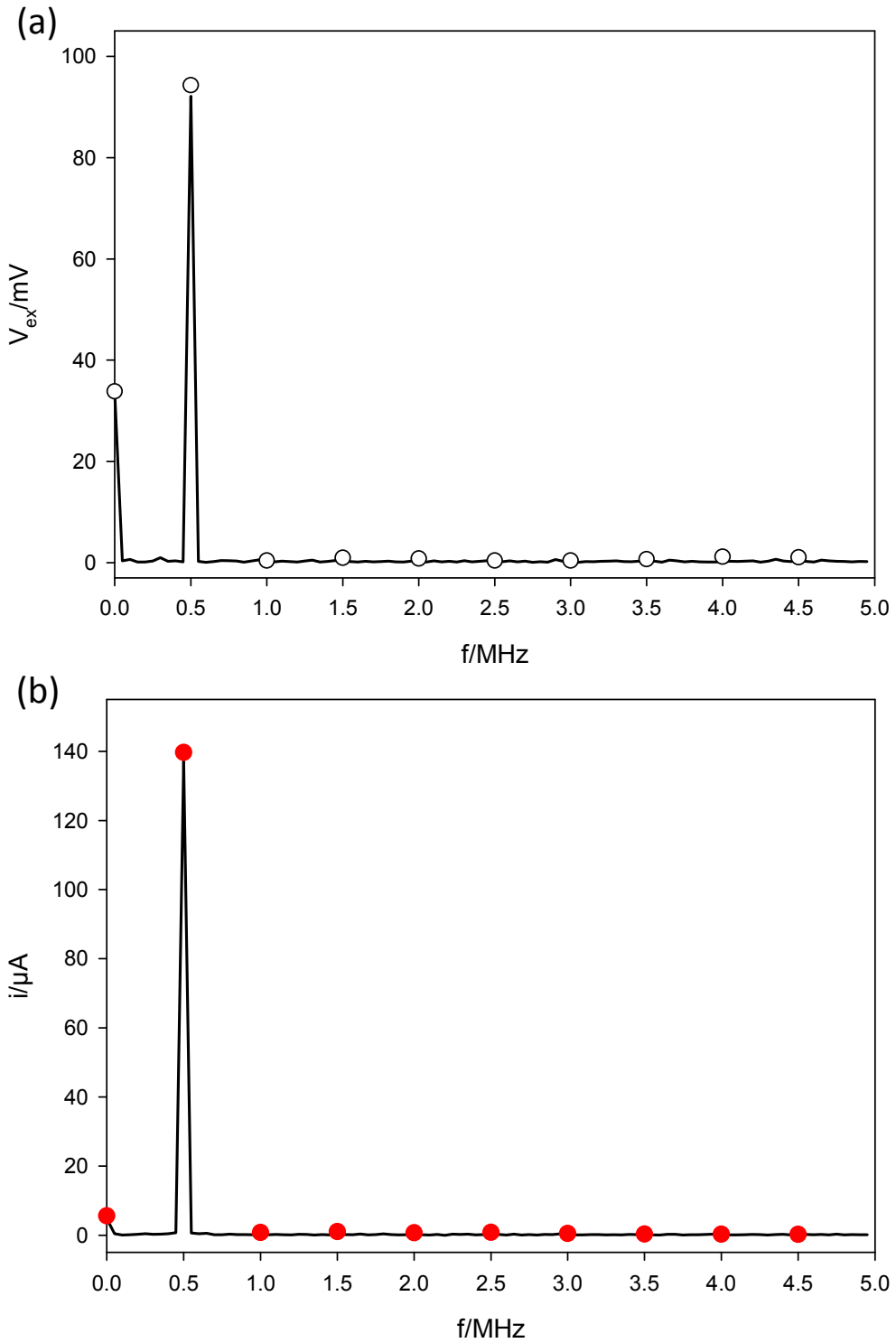

Figure S2. Plots showing an example of the FFT analysis of the data. (a) shows the results for the excitation signal (V_{ex}) and (b) the resulting current signal (i) as a function of frequency (f). Here a 2 µs window (O, ● for V_{ex} and i respectively) has been analysed and for completeness a 20 µs window (—). In all cases the analysis shows the 500 kHz signal as the dominant component as expected.

Note that in this case the analysis for a 20 point (corresponding to 2 µs, ●, ○) and a 200 point (corresponding to 20 µs, ▬) window are shown. The analysis shows that this signals are centred on 500 kHz as expected. The magnitude of the 500 kHz component of the applied voltage perturbation and the corresponding current component are then used to enable the appropriate parameter to be calculated. For example, the FFT results are used to calculate the impedance (*Z*) of the electrode. Figure S3 shows how the extracted DC current (I_F, extracted from the 0 Hz data point), corrected phase angle (between the voltage and current signals) and impedance (*Z*) vary as a function of time as the electrode was exposed to cavitation. In order to correct for instrumental limitations, a set of dummy cells were investigated. These were chosen to closely mimic the appropriate uncompensated resistance and capacitance of the electrode. This analysis showed that there was a systematic underestimation in the measured phase angle (θ). This systematic shift was found to be 9° for the AD817 amplifier and conditions employed. This value was used to correct the phase angle (and is shown in figure S3 as '$\theta+\theta_s$', where 'θ' is the measured angle and 'θ_s' is the 9° instrumentational error).

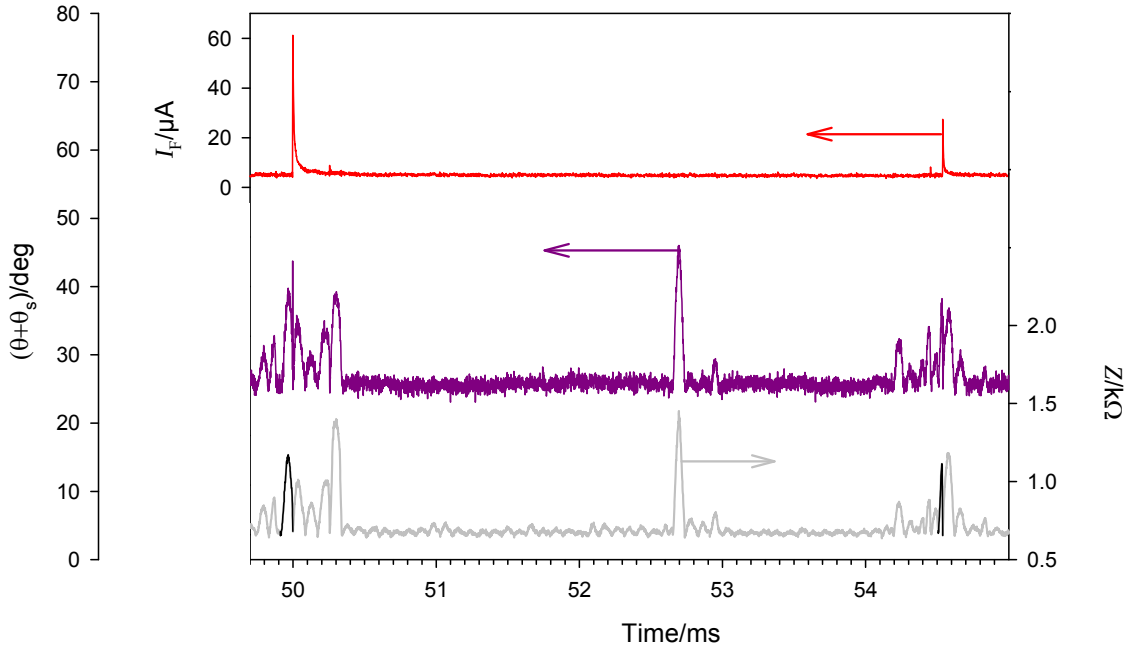

Figure S3. Plot showing the Faradaic current (I_F, ▬), corrected phase angle ($\theta+\theta_s$, ▬) and impedance (*Z*, ▬) for an aluminium electrode exposed to cavitation. All experimental details as shown in the main text. Note the two transients in this data set which cause surface erosion are highlighted in the impedance data (▬).

It is assumed that the Faradaic impedance of the system (assuming a Randles circuit arrangement) is much larger than the other components and so for simplicity we use a simple resistor capacitor model to depict the electrochemical cell under the conditions and frequency regime employed. This assumption is supported by the observation that the DC current passed was < 100 µA at all times indicating a relatively large Faradaic impedance compared to the other components of the system (for example the uncompensated resistance of the electrode was < 2 kΩ at all times). The impedance of the electrode system and the phase angle between the voltage and current component were used to extract the values of the uncompensated resistance and the electrode capacitance.

A 100 mV zero-to-peak voltage excitation was deployed in the cavitation erosion/corrosion experiments. This was necessary to ensure that the data extracted from the FFT was accurate and stable during the erosion/corrosion transients. The values of the uncompensated resistance and apparent electrode capacitance determined using this high-speed approach were compared to measurements performed on a commercial electrochemical workstation (specifically a Biologic SP150 with an inbuilt impedance analyser). Figure S4 shows a conventional Nyquist plot for an aluminium 250 µm diameter electrode. Comparing the impedance plots obtained using a 100 mV and a 10 mV zero-to-peak excitation (see figure S4), it is apparent that the difference in the impedance recorded over this range is relatively small particularly at high frequency (relevant to the cavitation work) regime studied. Finally, there is reasonable agreement between the data obtained for the commercial system (see figure S4, ●, ○) and that for the high-speed system (see figure S4, ●).

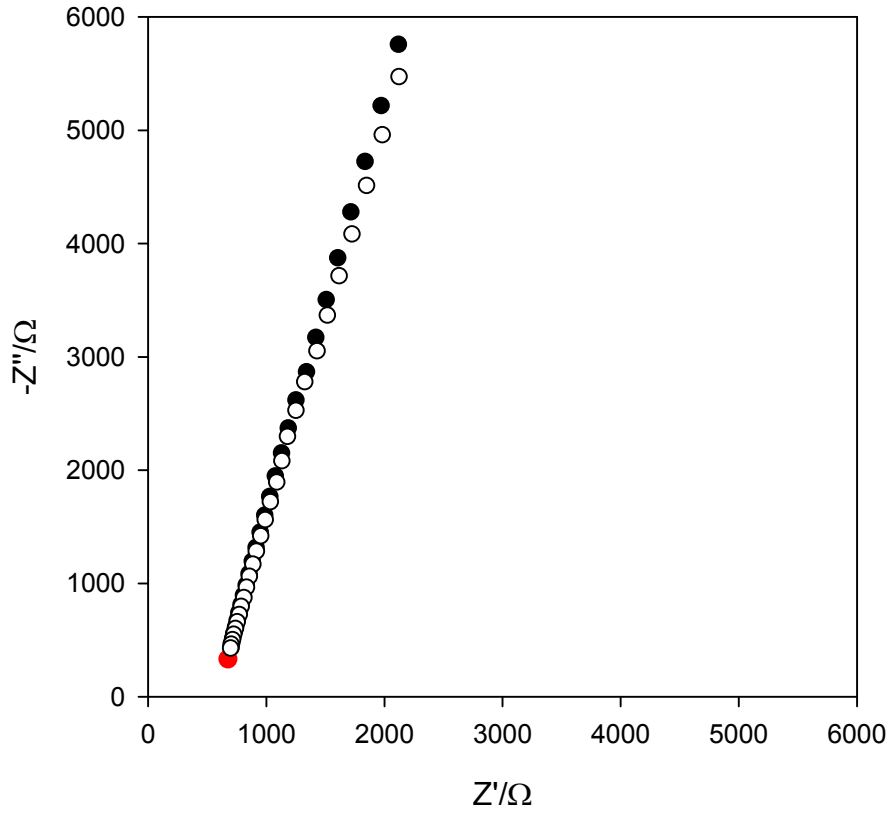

Figure S4. Nyquist plot obtained from a commercial impedance system (Biologic SP150) for a 250 µm diameter aluminium disk in 0.2 mol dm^{-3} Na_2SO_4 at ~26 °C. The data was obtained at 0 V *vs.* the stainless steel reference/counter employed. The applied zero-to-peak voltage perturbations were 10 mV (○) and 100 mV (●). The data was recorded for a frequency range of 10-623 kHz. The single point from the instrumentation used in the cavitation work is also shown for comparison (●).

This suggests that the method employed, although non-ideal, provides a reasonable estimate of the real uncompensated resistance and the apparent electrode capacitance and allows for the dynamic experiments described in the main text to be possible. Finally, the complexity of the system may force the values of R_u and C_a to be correlated, particularly considering the single high frequency measurement employed. This may result in an imperfect separation of R_u and C_a. This is being investigated at this time.